

For many purposes  $\Delta E$  can be treated in terms of an effective mass

$$m_\omega = m(1 + \lambda), \quad (1.3.17)$$

where

$$\lambda = -\frac{\partial \Delta E}{\partial \omega}, \quad (1.3.18)$$

is the *mass enhancement factor*, while

$$Z_\omega = m/m_\omega,$$

measures the single-particle content (discontinuity) at the Fermi energy.

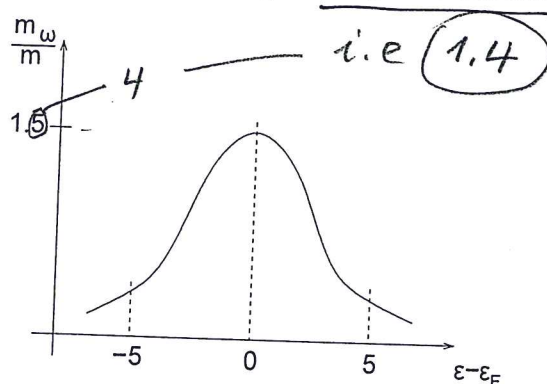
Consequently, Eq.(1.3.14) can be rewritten as

$$\left( -\frac{\hbar^2}{2m^*} \nabla_r^2 + U'_H + iW(\omega) \right) \varphi_j(\vec{r}) = \varepsilon_j \varphi_j(\vec{r}), \quad (1.3.19)$$

with

$$m^* = \frac{m_k m_\omega}{m}. \quad (1.3.20)$$

and  $U'_H = (m/m^*)U$  and similarly for  $W'$ . Because  $\lambda \approx 0.4$  (i.e. the dressed single-particle  $m_\omega$  is heavier than the bare nucleon, as it has to carry a phonon along or, better, move in a cloud of phonons),  $m^* \approx 1$  and  $Z_\omega \approx 0.7$ . Furthermore, due to the fact that  $\hbar\omega_a \approx 2 - 2.5 \text{ MeV}$ , the range of single-particle energy  $E = \varepsilon - \varepsilon_F$  over which the particle-vibration coupling process displayed in Fig.1.3.2 is effective is  $\approx \pm 2\hbar\omega_a \approx 4 - 5$  around the Fermi energy (see Figs.1.3.3 and 1.3.4)



✓ Figure 1.3.3: Schematic representation of the  $\omega$ -mass as a function of the single-particle energy.

It is of notice that  $\Delta E_j$  (Eq.(1.3.15)) indicates the shift of the centroid of the "dressed" single-particle state due to the coupling to the intermediate (more complex states) doorway states  $\alpha' \equiv (\nu', \alpha)$ , while  $\Gamma = 2W$  measures the energy range over which the single-particle state spreads due to the coupling (see Fig.1.3.5).

complicated

is the only correct picture to describe the coupling of a nucleon moving in a single-particle state with more complicated configurations<sup>34</sup>. However, such a description is quite involved. On the other hand, to account for the change of the centroid energy and of its spreading width in terms of an *optical potential*  $\Delta E + iW$  is very economic and convenient. In any case  $\Gamma$  measures the range of energy over which the "pure" single-particle state  $|\alpha\rangle$  spreads due to the coupling to the more complicated doorway states  $|\alpha'\rangle$ . In other words, a stationary state

$$\varphi_\nu(\vec{r}_i t) = e^{\frac{i\omega t}{\hbar}} \varphi_\nu(\vec{r}), \quad (1.3.24)$$

has a probability density

$$\int d^3 r |\varphi_\nu(\vec{r}_i t)|^2 = \int d^3 r |\varphi_\nu(\vec{r})|^2 = 1, \quad (1.3.25)$$

which does not depend on time. That is, if at  $t = 0$ , the probability that the particle is in a state  $\nu$  is 1, it will have this probability also at  $t = \infty$ , implying an infinite lifetime. If however,

$$\omega = \varepsilon_\nu^{(0)} + \Delta E_\nu(\omega) + i \frac{\Gamma}{2}(\omega), \quad = \varepsilon_\nu + i \frac{\Gamma_\nu}{2}(\omega) \quad , (\varepsilon_\nu = \varepsilon_\nu^{(0)} + \Delta E_\nu)$$

then

$$\varphi_\nu(\vec{r}_i t) = e^{i \frac{\varepsilon_\nu t}{\hbar}} e^{-\frac{\Gamma_\nu t}{2\hbar}},$$

and

$$\int d^3 r |\varphi_\nu(\vec{r}_i t)|^2 = e^{-\frac{\Gamma_\nu t}{\hbar}}, \quad (1.3.26)$$

implying a lifetime of the single-particle state

$$\tau = \hbar / \Gamma. \quad (1.3.27)$$

One may ask, how it is possible that the coupling to complicated (but still simple) states like  $|\alpha'\rangle = |n_\alpha = 1, \nu'\rangle$  can explain the full damping of a single-particle state  $8-10\text{ MeV}$  from the Fermi energy  $\varepsilon_F$ , where the density of levels of all types is very large. This is because the Hamiltonian given in Eq. (1.3.1) contains all the basic physics to describe the ~~dressed~~ single-particle motion as far as surface modes are concerned (within this context see the discussion carried out following Eq. (1.3.13)). Any coupling to more complicated states will go through a hierarchy of couplings. In

<sup>34</sup>To be noted that if we spread the strength of a stationary quantal state in a number of doorway stationary states over an energy range  $\Gamma$ , and set all components in phase at  $t = 0$ , they will essentially be out of phase at  $t = \tau = \hbar/\Gamma$ . In other words, each component will behave independent of each other and the original correlated state, created at  $t = 0$  with probability 1 essentially ceases to exist at  $t = \tau$ . This does not imply that each of the incoherent members of the original coherent state cannot  $\gamma$ -decay at a much later stage. It is through such a process ( $\Gamma_\gamma \sim 1/10^{15}\text{ sec}$ ) as well as through particle decay ( $\Gamma \sim 1/10^{18}\text{ sec}$ ) that each (compound) state carrying a fraction of the giant resonance (e.g. the GDR) acquires a finite lifetime.

needed

$(\Gamma_{\alpha_0}/\Gamma \lesssim 10^{-2})$ , see e.g. Bortignon et al (1998)

book Giant Resonance

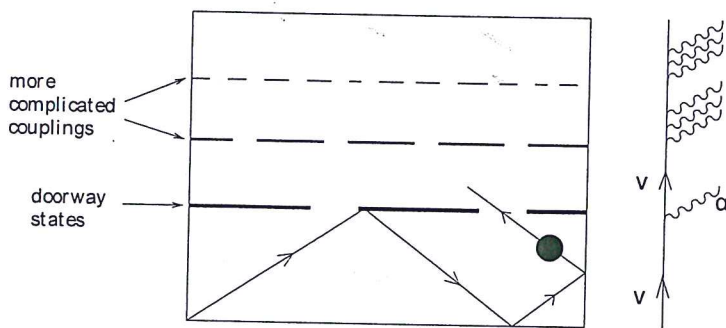


Figure 1.3.6: Schematic representation of the different levels of couplings leading to the damping of a single-particle state. It is essentially the first doorway coupling which controls the probability the ball (black dot) reflecting elastically on the walls of the box has to remain in the first compartment.

*other words, the variety of couplings, particularly all couplings, even the most complicated, should go through the coupling to states of type  $|\nu', \alpha'\rangle$ . In other words,  $|\alpha'\rangle$  is a doorway state (see Fig. 1.3.6)<sup>35</sup>.*

In the nuclear case, *the doorway coupling provides the basic breaking* of the single-particle motion, while higher-order couplings essentially only *fill in valleys* (see Fig. 1.3.7). *In other words, the quantity  $\Gamma$  (Eq. (1.3.27)) gives the range over which the single-particle state is spread due to all the couplings.*

In the case of the  $1s_{1/2}$  orbital of  $^{40}\text{Ca}$  ( $\epsilon - \epsilon_F = -8 \text{ MeV}$ ), simple estimates<sup>36</sup> lead to  $\bar{V}^2 \approx 0.3 \text{ MeV}$  for the coupling to an  $L = 2$  phonon, and  $n(\epsilon_F) \approx 2 \text{ MeV}^{-1}$ . Consequently

$$\Gamma \approx 4 \text{ MeV}, \quad (1.3.28)$$

in overall agreement with the experimental findings (see Fig. 1.3.8).

The result given in Eq.(1.3.28) is a particular example of the general (empirical) result (see Fig. 1.3.4)<sup>37</sup>.

$$\Gamma_{sp}(E) = \begin{cases} 0.5E & E > 5 \text{ MeV}, \\ 0 & E \leq 5 \text{ MeV}, \end{cases} \quad (1.3.29)$$

where

$$E = |\epsilon - \epsilon_F|. \quad (1.3.30)$$

### 1.3.2 Induced interaction

A nucleon at the Fermi energy which creates, by bouncing inelastically off the nuclear surface a collective mode, has no other choices than to continue on such

<sup>35</sup>Feshbach (1958).

<sup>36</sup>Mahaux, C. et al. (1985)

<sup>37</sup>Bertsch et al. (1983)

Simple estimates of this induced interaction leads, in the case of  $^{208}\text{Pb}$ , to values of the matrix element for pairs of particles coupled to angular momentum  $J^\pi = 0^+$  of  $-1.5\text{ MeV}$ , when summed over all the different multipolarities  $\alpha$  ( $L^\pi = 2^+, 3^-, 5^-$ , label  $\alpha$  in Fig. 1.3.9). The fact that one considers particles coupled to angular momentum zero is because the associated orbitals have maximum overlap, thus profiting at best from the (pairing) interaction<sup>38</sup>. In the case of two particles outside closed shell one would then expect the ground state to display, due to this mechanism, a correlation energy of about 1.5 MeV larger than that predicted by the independent particle model (see Fig. 1.3.10), and about half the value if one takes into account that  $Z_\omega \approx 0.7$  for each of the interacting particles. From this result one can conclude that the pairing interaction induced by the process depicted in Fig. 1.3.9, is likely to renormalize in an important way the bare,  $NN(^1S_0)$ —short range pairing interaction.

## 1.4 Coupling between elementary modes

Let us now return to the subject of the finite overlap existing between the elementary modes of nuclear excitation. That is, to the fact that one is working in a basis of states which contains already much of the physics one likes to describe, but which has the shortcoming of being overcomplete. An orthogonalization protocol, like a generalized Gram–Schmidt procedure, but leading to an effective field theory, where the different modes melt to some extent together, is called for (see Sect. 1.5).

A similar situation is found in the case of transfer processes in general, and of two-nucleon transfer in particular. One can work out the associated transfer amplitude by orthogonalizing, making use of second order perturbation theory, the single-particle wavefunctions of target and projectile. This can be done both within the semiclassical approximation (Sect. 5.C, see also Sect. 1.6) and DWBA (Sect. 3.2 and 5.2).

Because the coupling between elementary modes of excitation is proportional to their overlap, and in keeping with the fact that mean field theory is the natural starting point of nuclear structure calculations, overcompleteness of the basis is tantamount to the appearance of linear couplings between quasiparticles and collective modes (see Sect. 1.3 and App. 1.B in the case of surface modes and Sect. 1.7 in the case of surface and of pairing modes; see also Fig. 1.7.9), which in the case of reactions corresponds to the recoil modes (see e.g. Figs. 1.1.2 and 1.1.3, 5.C.1 and 5.C.2; see Fig. 4.1.1 in the case of one-particle transfer).

and Figs.

see also

App. 1.D)

Basis orthogonalization thus implies the diagonalization of the associated particle-vibration coupling Hamiltonian  $H_c$ . The rules to do so have been cast into a graphical effective field theory, namely the Nuclear Field Theory (NFT, see Sect. 1.7). In it, the free fields are to be calculated in the HF (HFB) approximation (particle (quasiparticle)) and in the RPA (QRPA) (vibrations). These elementary modes of excitation interact through the particle–vibration coupling vertices, while particles

<sup>38</sup>Note that quadrupole pairing correlations are also important.

and  
4.1.1

can also interact through four-point vertices ( $NN$ -bare interaction) (Figs. 1.7.9 (a) and (b)).

The NFT rules for evaluating the effect of these couplings between fermions and bosons involve a number of restrictions concerning initial and intermediate states as compared with the usual rules of perturbation theory that are to be used in evaluating the effect of the original (bare) nucleon-nucleon interaction properly renormalized by the exchange of vibrations between nucleons. This is in keeping with the fact that the collective modes contain, from the start, the correlations arising from forwards and backwards going particle-hole ( $\beta = 0$ ) as well as particle-particle ( $\beta = +2$ ) and hole-hole ( $\beta = -2$ ) bubbles. Furthermore, this is because these (quasi) bosons are not elementary but composite fields, made out of pairs of fermions, and thus subject to the Pauli principle (see Sect. 1.8).

The general validity of NFT rules have been demonstrated by proving the equivalence existing, to each order of perturbation theory, between the many-body finite nuclear system propagator calculated in terms of Feynman diagrams involving only the fermionic degrees of freedom i.e. explicitly respecting Pauli in a complete and not overcomplete basis, and the propagator constructed in terms of Feynman diagrams involving fermion and phonon degrees of freedom (NFT Feynman diagrams) in the case of a general two-body interaction and an arbitrary distribution of single-particle levels<sup>39</sup>.

Concerning the actual embodiment of NFT one can recognize the practical difficulties of respecting the corresponding rules. This is in keeping with the fact that there is not a single bare, well behaved, low- $k$   $NN$ -force (eventually with  $3N$  and higher order corrections) with which it is possible to generate a mean field (Eq. (1.2.3), also Fock potential see Fig. 1.2.1 (c)) to determine the single-particle states and, by introducing a periodic time-dependence with the constrain

$$\delta U(r) = \int d\mathbf{r} \delta\rho(\mathbf{r}') v(|\mathbf{r} - \mathbf{r}'|), \quad (1.4.1)$$

calculate the collective modes associated with the variety of particle-hole ( $\beta = 0$ ; density, spin, isospin, etc.) and pairing ( $\beta = \pm 2$ ; monopole and multipole pair addition and pair subtraction) modes. If this was possible, one could then diagonalize, within the framework of NFT and to the desired order of perturbation, also infinite order, the resulting particle-vibration couplings, and thus obtain renormalized quantities which can be directly compared with the data. In other words, a real physical *ab initio* calculation could be done, resulting in a single, common ground state which, corrected with the corresponding homogeneous ZPF lead eventually to the "exact" ground state as well as to properly dressed modes and pairing interaction (see Sect. 1.7).

On the other hand, empirical implementation of the NFT rules (empirical renormalization)<sup>40</sup> have been carried out, making use of the bare Argonne  $v_{14}$  poten-

<sup>39</sup> Bès and Broglia (1975); see also Baranger (1969) and the lecture notes of McFarlane (1969)

<sup>40</sup> Broglia et al. (2016), *Phys. Rev. C* 94, 054312

b) Bohr (1964)

Computer Rendus  
bibliografie generale  
add to that  
of Ch. 2

Similar, but more accurate results are obtained by freely parametrising the bare potential so that the observed particle reproduce the data experimentally.

*(From this example one can see)*

tial, and of Skyrme like SLy<sup>41</sup> forces (or Saxon-Woods parametrizations and  $m_k \approx 0.7m$ ) to determine the mean field and spin vibrational channels, and of multipole-multipole forces with self-consistent coupling constants for the variety of density vibrational channels.

The resulting predictions are, as a rule, able to provide, together with the specific reaction software, in particular COOPER and SINGLE, an overall account of "complete" sets of experimental data, obtained with the help of Coulomb, inelastic and one- and two-nucleon transfer data, able to map out the nuclear structure and reaction landscape<sup>42</sup>. Summing up, the nuclear structure description given by the elementary modes of nuclear excitation approach within the framework of NFT, provides a unified description of the variety of observables. At the same time, each cross section or transition probability is connected to essentially all others. This is the reason why we bring together pair (as well as one-particle) transfer with the rest of the observables both for open-shell nuclei along the stability valley, as well as for exotic closed shell nuclei, to demonstrate that: 1) it is possible to predict, with few (~~less~~) parameters, most of them strongly constrained by empirical input, the experimental findings within a 10% level of accuracy; 2) that the nuclear landscape, as it emerges from NFT based on elementary modes of excitation and of their interweaving through the particle-vibration coupling, is well funneled (Fig. 1.4.1), its minimum essentially coinciding with the global minimum resulting from the empirical renormalization choice of basic quantities ( $m_k$ , strength bare pairing, properties of few low-lying collective modes ( $p - h$ ) and pairing vibrations). An important proviso concerning the above parlance is that one considers a group of homogeneous nuclei like e.g. open shell spherical superfluid nuclei (like the Sn isotopes), or nuclei around closed shells (like  $^{208}\text{Pb}$ ,  $^{12}\text{Be}$ ,  $^{11}\text{Li}$ , etc.).

*for details see Sect. ?? In connection with light exotic halo nuclei we refer to Sect. 1.9 of the present chapter and to Sect. 4.2.2. A-A from handwritten pp, (36)<sub>a</sub> and (36)<sub>b</sub>*

## 1.5 Non-orthogonality

The ground state of  $^{210}\text{Po}_{126}$  can be viewed as the proton pair addition mode of the doubly closed shell nucleus  $^{208}\text{Pb}_{126}$ , mode displaying  $J^\pi = 0^+$  and  $\beta = +2$  (transfer-) quantum numbers. Within this framework  $^{209}\text{Bi}_{126}$  is expected to be a *bona fide* proton single-particle system ( $\beta = +1$ ), in which the  $g_{7/2}$ ,  $d_{5/2}$ ,  $h_{11/2}$ ,  $d_{3/2}$  and  $s_{1/2}$  valence orbitals are occupied, the odd proton occupying, in the ground state, a substate of the  $h_{9/2}$  orbital.

This picture can be specifically probed through one-proton stripping and pick up reactions, e.g. with the help of  $^{210}\text{Po}(t, \alpha)^{209}\text{Bi}$  and  $^{208}\text{Pb}({}^3\text{He}, d)^{209}\text{Bi}$  transfer processes<sup>43</sup>. The pick-up reaction cross section is, in the case of e.g. the states

<sup>41</sup>Chabanat et al. (1997).

<sup>42</sup>Idini et al. (2015); Idini, A. et al. (2014); Potel, G. et al. (2013).

<sup>43</sup>It is of notice that in the present case, as well as in Sect. 1.7, and at variance with the rest of the monograph, use will be made, for the sake of being didactic, of spectroscopic factors, see end of Sect. 2.1.

b Barranco et al (2017)  $^{11}\text{Be}$

(A) Let us shortly dwell on Fig. 1.4.1. The concept of a well funnelled energy landscape is easy to understand in the case in which the number of particles  $N \rightarrow \infty$  (thermodynamic limit). For example, a swing will have a very simple and well funnelled potential energy landscape. A similar concept which still retains the <sup>classical</sup> viewpoint, but now referred to the free energy of large molecules, has been used in an attempt to describe protein folding. (Wolynes PNAS, whole PNAS volume, P. Wolynes (2016)). One has to hypothesize that the results of all atom, explicit solvent classical molecular dynamic simulations can be interpret in terms of a somewhat rugged, but still well funnelled free energy landscape.

When we <sup>see</sup> such behaviour in the nuclear case, even not so well defined, and somehow imperfect, we recognize that the nucleus is, after all, not macroscopic. ~~and the~~ Concepts strictly valid for  $N \rightarrow \infty$  are strongly renormalized by quantal finite size effects, in particular zero point fluctuations [ZPF, Fig. 1.4.2].

\*\*) This nuclear result in turn, may be precious to shed light into the physics which is at the basis of protein folding. We like it or not, these <sup>quantal</sup> systems are quantal, and the associated fluctuations are likely to play an important role in fleeting transition states.

\* P. Wolynes, Moments of excitement, Science 352, 150 (2016)  
P. Wolynes, whole PNAS volume (2016)

~~Proceedings  
of the National Academy  
of Sciences U.S.A.  
Editor: P. Wolynes~~

~~Volente et alentis~~

Proceedings of the National Academy  
of Sciences P. Wolynes editor

(continuation of footnote p. 36a)

(36)  
b

The fact that the average transit times and the shapes of the transit-time distributions agree well with the simplest one-dimensional theory may only reflect the large uncertainties of the tunneling probabilities, small changes in the barrier's parameters compensating for the lack of quantal phenomena. Within this context one is reminded of  $\alpha$ - and exotic-decay.

In other words, it is likely that the "imperfect" nature of the nuclear structure landscape funnel, an example of which is shown in Fig 1.4.1 embodies more accurately the physics of quantal, many-body systems than that of a smooth, more pedagogical construct essentially based on potential energy, even with the entropic contribution (free energy). This is in keeping with the fact that the interaction terms (potential energy) of the Hamiltonian contain the last vestiges of Newton's conception of force or, causation, being thus too much anchored to classical mechanics.

Handwritten see pp. (37a + 37b)  
Kob. 7/6/16

(A) p. 36  
ch. I

Within this context we refer to Fig. 1.4.2, and to the fact that the nuclear ground state (nuclear vacuum), virtually contains all the physics of the system, as demonstrated by acting with the variety of external field which exhaustively probes it.

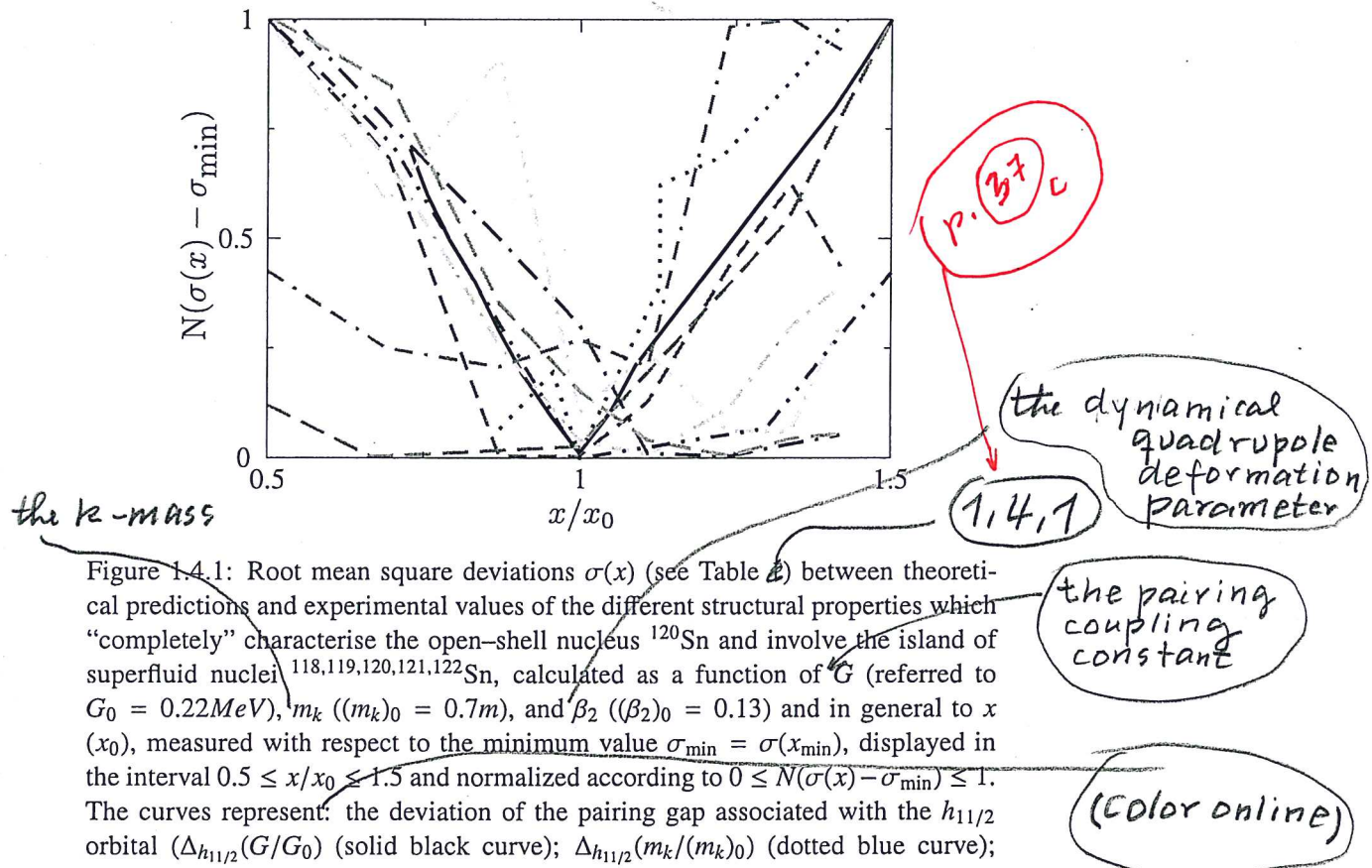
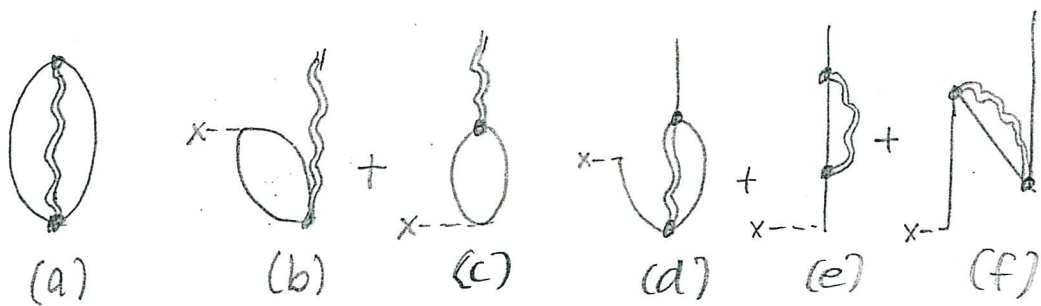


Figure 1.4.1: Root mean square deviations  $\sigma(x)$  (see Table 1) between theoretical predictions and experimental values of the different structural properties which “completely” characterise the open-shell nucleus  $^{120}\text{Sn}$  and involve the island of superfluid nuclei  $^{118,119,120,121,122}\text{Sn}$ , calculated as a function of  $G$  (referred to  $G_0 = 0.22\text{MeV}$ ),  $m_k ((m_k)_0 = 0.7m)$ , and  $\beta_2 ((\beta_2)_0 = 0.13)$  and in general to  $x$  ( $x_0$ ), measured with respect to the minimum value  $\sigma_{\min} = \sigma(x_{\min})$ , displayed in the interval  $0.5 \leq x/x_0 \leq 1.5$  and normalized according to  $0 \leq N(\sigma(x) - \sigma_{\min}) \leq 1$ . The curves represent: the deviation of the pairing gap associated with the  $h_{11/2}$  orbital ( $\Delta_{h_{11/2}}(G/G_0)$  (solid black curve);  $\Delta_{h_{11/2}}(m_k/(m_k)_0)$  (dotted blue curve);  $\Delta_{h_{11/2}}(\beta_2/(\beta_2)_0)$  (dashed green curve)); the deviation of the quasiparticle spectrum ( $E_{qp}(G/G_0)$  (dashed brown curve);  $E_{qp}(\beta_2/(\beta_2)_0)$  (dash-dotted green curve)); the deviation of the  $h_{11/2} \otimes 2^+$  multiplet splitting  $E_{h_{11/2} \otimes 2^+}(\beta_2/(\beta_2)_0)$  (dash-dotted purple curve); the deviation of the centroid position of the  $d_{5/2}$  strength function  $S_{d_{5/2}}(\beta_2/(\beta_2)_0)$  (dash-dotted cyan curve); the deviation of the width of the  $d_{5/2}$  strength function  $S_{d_{5/2}}(\beta_2/(\beta_2)_0)$  (dash-dotted pink curve); the deviation of the quadrupole transition strength  $B(E2)(\beta_2/(\beta_2)_0)$  (dashed orange curve). For details see Idini et al. (2015). The remarkable feature of the present figure is the fact that, in spite of the fluctuations of the results typical of finite many-body systems, clearly defines a funnel in which all minima fall within a narrow window of  $x/x_0$  values ( $1 \pm 0.2$ ). This is a novel and unexpected result, which can be considered as an emergent property of a description of structure and reactions carried out in a basis of elementary modes of excitations, interacting through the PVC vertices according to the NFT rules.

Fig. 1.4.2 Version April 26, 2016

(37)  
a

1.4.2

Caption to Fig. ~~1.10~~**bold face**

(diagrams)

Schematic representation of the NFT (str) at the basis of the characterization of a superfluid nucleus like e.g.  $^{120}\text{Sn}$ . (a) Nuclear structure (NFT(s)). Zero point fluctuations (ZPF) characterizing the nucleus ground state. Continuous lines describe quasiparticle states, double wavy curves correlated ZPF vibrational modes. Because  $\alpha_v^+ = \alpha_v^-$  at  $-V_0$ , at  $V_0$  these modes encompass both particle-hole ( $^{(ph)}$ ) like vibrations, e.g. surface quadrupole vibrations, as well as correlated ( $^{(pp)}$ ) and ( $^{(hh)}$ ) monopole and multipole graining vibrations. In lowest order in the particle-vibration coupling vertices diagram (a) contains all the physics characterizing the nucleus  $^{120}\text{Sn}$ , in keeping with the fact that each single elementary mode of excitation, namely each excited state of the system is virtually present in the nuclear vacuum (ground state). In fact (a) represents the actual many-body ground state of the system. This can be

København 7/06/16 (37)<sup>b</sup>

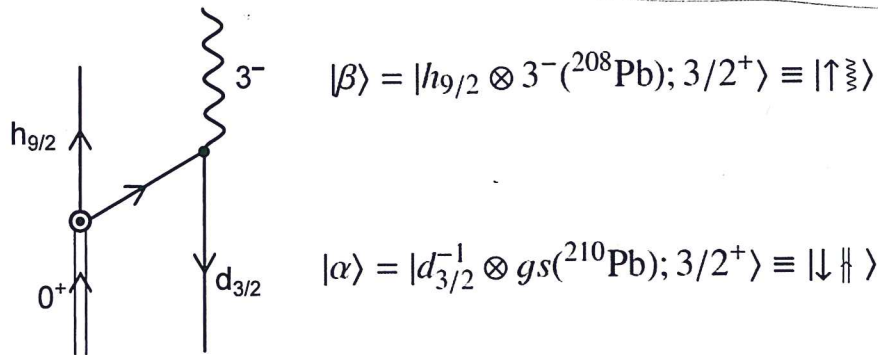
demonstrated by probing the system with  
a variety of external fields: (b), (c) mag-  
netic and two-nucleon transfer processes.  
(d)-(f) one-nucleon transfer reactions.

In highest orders, Pauli principle  
between the quasiparticles considered  
explicitly (continuous curves) and those  
participating in the mode (double wavy  
lines) is taken care of. As a consequence  
pure ZQP excitations are eliminated  
and little collective ZQP states are  
essentially screened out.

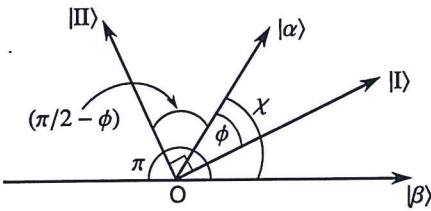
intervene: to interfere with the outcome or course especially  
of a condition or process  
intervenire to come between

Observables	SLy4	$d_{5/2}$ shifted	Opt. levels
$\Delta$	10 (0.7%)	10 (0.7 %)	50 (3.5 %)
$E_{qp}$	190 (19%)	160 (16%)	45 (4.5 %)
Mult. splitt.	50 (7%)	70 (10%)	59 (8.4 %)
$d_{5/2}$ strength (centr.)	200 (20%)	40 (4%)	40 (4%)
$d_{5/2}$ strength (width)	160 (20%)	75 (9.3%)	8 (1%)
$B(E2)$	1.4 (14%)	1.34 (13%)	1.43 (14%)
$\sigma_{2n}(p, t)$	0.6 (3%)	0.6 (3%)	0.6 (3%)

Table 1: Root mean square deviation  $\sigma$  between the experimental data and the theoretical values expressed in keV for the pairing gap, quasiparticle energies, multiplet splitting, centroid and width of the  $5/2^+$  low-lying single-particle strength distribution. In single-particle units  $B_{sp}$  for the  $\gamma$ -decay ( $B(E2)$  transition probabilities) and in mb for  $\sigma_{2n}(p, t)$ . In brackets the ratio  $\sigma_{rel} = \sigma/L$  between  $\sigma$  and the experimental range  $L$  of the corresponding quantities: 1.4 MeV ( $\Delta$ ), 1 MeV ( $E_{qp}$ ), 700 keV (mult. splitting), 1 MeV ( $d_{5/2}$  centroid), 809 keV (=1730- 921) keV ( $d_{5/2}$  width), 10  $B_{sp}$  ( $B(E2)$ ), 2250 mb ( $\sigma_{2n}(p, t)$ ), is given (for details see [109]). Jain et al. (2015), also Fig. 1.10.1



✓ Figure 1.5.1: NFT diagram describing one of the most important processes coupling the  $2p - 1h$  states  $|\alpha\rangle$  and  $|\beta\rangle$  (see Eqs. (1.5.1) and (1.5.2)), product of bare elementary modes of excitation consisting in the  $^{208}\text{Pb}$ ,  $0^+$  pair addition mode and the  $d_{3/2}$  proton hole state, and of the lowest octupole vibration of  $^{208}\text{Pb}$  and of a proton moving in the  $h_{9/2}$  orbital.



✓ Figure 1.5.2: Schematic representation of the  $3/2^+$  states entering the NFT calculation of the process displayed in Fig. 1.5.1. The basis state  $|\alpha\rangle$  carries the full  $(t, \alpha)$  transfer strength ( $tr$ )  $\sigma^{tr}$ , while the basis state  $|\beta\rangle$  the full octupole ( $oct$ ) strength  $\sigma^{oct}$  (see Tables 1.5.1–1.5.3). The overlap between these states is  $\cos\chi$ . The physical states obtained through the (Feynman) diagrammatic “orthogonalization process” are denoted  $|I\rangle$  and  $|II\rangle$  (see Eqs. (1.5.3) and (1.5.4)).

$1/2^+(s_{1/2})$  and  $11/2^-(h_{11/2})$ , essentially consistent with a single peak displaying full  $(2j + 1)$  occupancy. On the other hand, two  $3/2^+$  states with essentially equal strength and exhausting the associated  $(2j + 1 (= 4))$  strength are observed. Furthermore, the four peaks mentioned above are essentially not excited in the stripping process (see Table 1.5.1). In an attempt to further clarify the structure of the two  $3/2^+$ , ~~referred~~ is made to the inelastic process  $^{209}\text{Bi}(d, d')$ . Both states are excited in the inelastic process, the associated angular distributions revealing the octupole character of such excitation (Tables 1.5.2 and 1.5.3).

use  
of

In keeping with the fact that the same experiment reveals a multiplet (septuplet) of states with centroid around 2.6 MeV and with summed  $L = 3$  inelastic cross section consistent with that of the lowest collective (2.615 MeV,  $B(E3)/B_{sp} \approx 32$ ) octupole vibration of  $^{208}\text{Pb}$ , one can posit that the two  $3/2^+$  states are a linear combination of the unperturbed (two particles)–(one hole)  $(2p-1h)$  states (see Fig.

	$E_x(\text{MeV})$	$S(t, \alpha)(2j + 1)$	$S(^3\text{He}, d)$
$3/2^+$	2.49	$1.8 \pm 0.3 (4)$	$< 0.01$
$3/2^+$	2.95	$2.2 \pm 0.3 (4)$	$< 0.01$
$1/2^+$	2.43	$1.8 (2)$	$< 0.02$
$11/2^-$	3.69	$10 (12)$	$< 0.05$

✓ Table 1.5.1: Single-particle strength associated with the single-particle transfer reactions  $^{210}\text{Po}(t, \alpha)^{209}\text{Bi}$  and  $^{208}\text{Pb}(^3\text{He}, d)^{209}\text{Bi}$  (see Bortignon, P. F. et al. (1977)).

1.5.1),

$$|\alpha\rangle = |d_{3/2}^{-1} \otimes gs(^{210}\text{Pb}); 3/2^+\rangle, \quad (1.5.1)$$

and

$$|\beta\rangle = |h_{9/2} \otimes 3^-(^{208}\text{Pb}); 3/2^+\rangle. \quad (1.5.2)$$

Because these states lie very close in energy they mix. According to NFT, the most important contribution to this mixing arises from the process given in Fig. 1.5.1. The resulting physical (mixed) states can be written as,

$$|I\rangle = -0.53|\alpha\rangle + 0.76|\beta\rangle, \quad (1.5.3)$$

and

$$|II\rangle = 1.02|\alpha\rangle + 0.80|\beta\rangle, \quad (1.5.4)$$

as resulting from the calculation of the diagram displayed in Fig. 1.5.1 to all orders of perturbation, with the help of Brillouin-Wigner perturbation theory (diagonalization of the corresponding effective Hamiltonian<sup>44</sup>). Let us now calculate the overlap  $O = \langle\alpha|\beta\rangle$  between the basis states  $|\alpha\rangle$  and  $|\beta\rangle$ , that is  $O = \cos\chi$  (see Fig. 1.5.2). Following this figure one can write,

$$\sqrt{\sigma_I^{tr}} = \cos\phi; \quad \sqrt{\sigma_{II}^{tr}} = \cos\left(\frac{\pi}{2} - \phi\right) = \sin\phi, \quad (1.5.5)$$

overlap  
Gregory  
use the  
same  
for  ${}^6\text{Li}$  ?

where

$$\sigma^{tr} = \sigma_I^{tr} + \sigma_{II}^{tr} = 1, \quad (1.5.6)$$

in keeping with the fact that the absolute cross sections of the states  $|I\rangle$  and  $|II\rangle$  are normalized in terms of the total cross section (see caption to Fig. 1.5.2).

In the same way

$$\sqrt{\sigma_I^{oct}} = \cos(\chi - \phi) = \cos\chi \cos\phi + \sin\chi \sin\phi, \quad (1.5.7)$$

<sup>44</sup>See p. 316 Bortignon, P. F. et al. (1977) and references therein.

40

	$E_x(\text{MeV})$	$\frac{\sigma(^{209}\text{Bi}(9/2^-;gs) \rightarrow ^{209}\text{Bi}(3/2^+;E))}{\sigma(^{208}\text{Pb}(gs) \rightarrow (3^-;2.615 \text{ MeV}))}$
3/2	2.49	$0.041 \pm 0.003$
3/2	2.95	$0.011 \pm 0.002$

Table 1.5.2: The total inelastic cross section  $\sigma^{oct}$  associated with the lowest octupole vibrational state of  $^{208}\text{Pb}$  can be written in terms of that associated with a single magnetic substate  $\sigma'$  as  $\sigma_{3^-}^{oct} = 7\sigma'$ . That associated with the multiplet  $(h_{9/2} \otimes 3^-)_{J^+}(J = 3/2 - 15/2)$  as  $\sigma_{3^-}^{oct} = 70\sigma'$ , in keeping with the fact that the  $h_{9/2}$  state has 10 magnetic substates. Thus, the strength associated with the 3/2 channel is  $4/70 = 0.057$  to be compared with the observed summed (percentage) strength  $0.053 \pm 0.005 (= (0.042 \pm 0.003) + (0.011 \pm 0.002))$  associated with the 2.45 MeV and the 2.95 MeV 3/2<sup>+</sup> states; see Bortignon, P. F. et al. (1977). **Table 4.11.**

	$E_n(\text{MeV})$		$\frac{\sigma(h_{9/2} \rightarrow 3/2^+)}{\sigma(0^+ \rightarrow 3^-)} (\%)$		$S(t, \alpha)$		$S(^3\text{He}, d)$	
	Theory	Exp	Theory	Exp	Theory	Exp	Theory	Exp
3/2	2.480	2.494	3.76	$4.2 \pm 0.3$	1.83	$1.8 \pm 0.3$	0.02	$< 0.01$
3/2	3.125	2.95	1.56	$1.1 \pm 0.2$	2.25	$2.2 \pm 0.3$	$10^{-5}$	$< 0.01$

Table 1.5.3: Summary of NFT predictions concerning the structure of the two lowest 3/2<sup>+</sup> state of  $^{209}\text{Bi}$ , in comparison with the experimental data (see Table 4.7 of Bortignon, P. F. et al. (1977)).

and

$$\sqrt{\sigma_{II}^{oct}} = \cos \left( \pi - \left( \frac{\pi}{2} - \phi + \chi \right) \right) = -\cos \left( \frac{\pi}{2} + (\phi - \chi) \right) = \sin \phi \cos \chi + \sin \chi \cos \phi. \quad (1.5.8)$$

Thus

$$\sqrt{\sigma_I^{oct}} = \cos \chi \sqrt{\sigma_I^{tr}} + \sin \chi \sqrt{\sigma_{II}^{tr}}, \quad (1.5.9)$$

and

$$\sqrt{\sigma_{II}^{oct}} = -\cos \chi \sqrt{\sigma_{II}^{tr}} + \sin \chi \sqrt{\sigma_I^{tr}}. \quad (1.5.10)$$

Multiplying the above relations by  $\sqrt{\sigma_I^{tr}}$  and  $\sqrt{\sigma_{II}^{tr}}$  respectively one obtains,

$$\sqrt{\sigma_I^{tr} \sigma_I^{oct}} = \cos \chi \sigma_I^{tr} + \sin \chi \sqrt{\sigma_I^{tr} \sigma_{II}^{tr}}, \quad (1.5.11)$$

and

$$\sqrt{\sigma_{II}^{tr} \sigma_{II}^{oct}} = -\cos \chi \sigma_{II}^{tr} + \sin \chi \sqrt{\sigma_I^{tr} \sigma_{II}^{tr}}, \quad (1.5.12)$$

Regarding the NFT of the above questions we refer to Sect. 1.7 as well as to App 1.c (Sect. 1.C.2).

In what follows we provide a simple, necessarily qualitative, estimate of the NFT.

### 1.6. COUPLING BETWEEN INTRINSIC AND RELATIVE MOTION

41

which, upon subtraction leads to the expression of the overlap

$$\cos \chi = \frac{\sqrt{\sigma_I^{tr} \sigma_I^{oct}} - \sqrt{\sigma_{II}^{tr} \sigma_{II}^{oct}}}{\sigma_I^{tr} + \sigma_{II}^{tr}}. \quad (1.5.13)$$

Making use of the values of Tables 1.5.1–1.5.3 (see also Fig. 1.7.10 (e) last column labeled *experiment*)<sup>45</sup> one obtains

$$\cos \chi = \frac{\sqrt{1.8 \times 4.2} - \sqrt{2.2 \times 1.1}}{4} = 0.298 \quad (1.5.14)$$

Simple estimates of the NFT prediction can be made making use of the relations<sup>46</sup>.

$$\langle I|I \rangle = (-0.53)^2 + (0.76)^2 - 2 \times 0.53 \times 0.75 \mathcal{O} = 1,$$

$$\langle II|II \rangle = (1.02)^2 + (0.80)^2 + 2 \times 1.02 \times 0.80 \mathcal{O} = 1,$$

and  $\langle I|II \rangle = -0.53 \times 1.02 + 0.76 \times 0.80 + (-0.53 \times 0.80 + 0.76 \times 1.02) \mathcal{O} = 0$  leading to  $\mathcal{O} = -0.18, -0.42$  and  $-0.19$  respectively and, thus, to the average value of  $-0.26$ . Of course, one can hardly expect to obtain the sign to agree with that of the NFT expression, as it is associated with a free choice of the axis of references (Fig. 1.5.2) (note also the fact that the quantities  $\sigma$  appearing above are well defined, while  $\sqrt{\sigma}$  is undetermined by an overall sign).

write a,  
in p. 39

write  
in  
p. 39

### 1.6 Coupling between intrinsic and relative motion

In what follows, we consider the reaction



within the framework of the semiclassical approximation<sup>47</sup>. In the center-of-mass system, the local Hamiltonian may be written

$$H = T_{aA} + H_a + H_A + V_{aA} = T_{bB} + H_b + H_B + V_{bA}, \quad (1.6.2)$$

in keeping with energy conservation. Within this context other, mixed, representations are possible.

One then solves the time-dependent Schrödinger equation

$$i\hbar \frac{\partial \Psi}{\partial t} = H\Psi, \quad (1.6.3)$$

with the initial conditions that the nuclei  $a$  and  $A$  are in their ground states, and where the relative motion is described by a narrow wavepacket of rather well defined impact parameter and velocity.

<sup>45</sup> See Table 4.7 of Bortignon, P. F. et al. (1977).

<sup>46</sup> see Table 4.6 Bortignon, P. F. et al. (1977).

<sup>47</sup> Broglia and Winther (2004) and references therein.

4, 5 and

We expand  $\Psi$  on (stationary) channel wavefunctions

$$\Psi = \sum_{\beta} c_{\beta} ((\mathbf{r}_{\beta} - \mathbf{R}_{\beta})) \Psi_{\beta} e^{-iE_{\beta}t/\hbar}, \quad (1.6.4)$$

where

$$\Psi_{\beta}(t) = \Psi_m^b(\xi_b) \Psi_n^B(\xi_B) \exp(i\delta_{\beta}). \quad (1.6.5)$$

The index  $\beta$  labels both the partition of nuclei ( $b, B$ ) as well as the quantal states of the two nucleons ( $m, n$ ).

The phase  $\delta_{\beta}$  is defined as

$$\delta_{\beta} = \frac{1}{\hbar} \left\{ m_{\beta} \mathbf{v}_{\beta}(t) \cdot (\mathbf{r}_{\beta} - \mathbf{R}_{\beta}(t)) - \int_0^t \left( U_{\beta}(\mathbf{R}_{\beta}(t')) - \frac{1}{2} m_{\beta} \mathbf{v}_{\beta}(t')^2 \right) dt' \right\}. \quad (1.6.6)$$

Where an extra phase has been added to eliminate, as far as possible, the diagonal matrix elements in the coupled equations. The phase factor  $\exp(i\delta_{\beta})$  acting on the channel wavefunction is essentially a Galilean transformation (see jagged "phonon" in the NFT reaction diagrams displayed in Figs. 4.1.1 (one-particle transfer) and 5.C.1 and 5.C.2 (two-particle transfer); see also Figs. 1.1.2 and 1.1.3).

The function  $c_{\beta}$  can be expressed as

$$c_{\beta} = a_{\beta}(t) \chi_{\beta}(\mathbf{r}_{\beta} - \mathbf{R}_{\beta}(t), t) \quad (1.6.7)$$

product of an amplitude  $a_{\beta}$  of asymptotic values ( $t = \pm\infty, 0$  or  $1$ ), and a normalized shape (wavepacket) function,  $R_{\beta}(t)$  being the relative motion elastic trajectory.

Properly combining the above quantities and making use of the time-dependent Schrödinger equation one obtains

$$i\hbar \sum_{\beta} \dot{a}_{\beta}(t) \langle \Psi_{\xi} | \Psi_{\beta} \rangle_{\mathbf{R}_{\xi}} e^{iE_{\beta}t/\hbar} = \sum_{\gamma} \langle \Psi_{\xi} | V_{\gamma} - U_{\gamma}(r_{\gamma}) | \Psi_{\gamma} \rangle_{\mathbf{R}_{\xi}} a_{\gamma}(t) e^{iE_{\gamma}t/\hbar}, \quad (1.6.8)$$

where

$$f(\mathbf{R}) = \langle \Psi_{\xi} | V_{\gamma} - U_{\gamma}(r_{\gamma}) | \Psi_{\gamma} \rangle_{\mathbf{R}} \quad (1.6.9)$$

are the formfactors, and

$$g(\mathbf{R}) = \langle \Psi_{\xi} | \Psi_{\beta} \rangle_{\mathbf{R}} \quad (1.6.10)$$

the overlaps between the intrinsic channel wavefunctions.

The coupled equations can be written in a more compact form by introducing the adjoint channel wavefunction

$$\omega_{\xi} = \sum_{\gamma} g_{\xi\gamma}^{-1} \Psi_{\gamma}, \quad (1.6.11)$$

where  $g^{-1}$  is the reciprocal of the overlap matrix

$$g_{\xi\gamma} = \langle \Psi_\xi | \Psi_\gamma \rangle. \quad (1.6.12)$$

Thus

$$(\omega_\xi, \Psi_\beta) = \delta(\xi, \beta), \quad (1.6.13)$$

and

$$i\hbar \dot{a}_\beta(t) = \sum_\gamma \langle \omega_\beta | V_\gamma - U_\gamma | \Psi_\gamma \rangle_{R_{\beta\gamma}} e^{(E_\beta - E_\gamma)t/\hbar} a_\gamma(t). \quad (1.6.14)$$

Consequently, the proper tunneling Hamiltonian is obtained by a basis orthogonalization process. These coupled equations, being first order in time, can be solved knowing the initial conditions at time  $t = -\infty$ ,

$$a_\gamma(-\infty) = \delta(\gamma, \alpha), \quad (1.6.15)$$

where  $\alpha$  labels the entrance channel, that is, the nuclei  $a$  and  $A$  in their ground state. The cross section for the reaction  $\alpha \rightarrow \beta$  is

$$\left( \frac{d\sigma}{d\Omega} \right)_{\alpha \rightarrow \beta} \sim |a_\beta(t = +\infty)|^2, \quad (1.6.16)$$

Let us now solve the coupled equations in first order perturbation theory. For this purpose we insert  $\delta(\gamma, \alpha)$  at the place of  $a_\gamma(t)$  obtaining

$$\begin{aligned} a_\beta(t) &= \frac{1}{i\hbar} \int_{-\infty}^t \langle \omega_\beta | V_\alpha - U_\alpha | \Psi_\alpha \rangle_{R_{\beta\alpha}(t)} \exp^{i(E_\beta - E_\alpha)t'/\hbar} dt' \\ &= \frac{1}{i\hbar} \int_{-\infty}^t dt' \langle \Psi_\beta | V_\alpha - U_\alpha | \Psi_\alpha \rangle_{R_{\beta\alpha}(t)} \exp^{i(E_\beta - E_\alpha)t'/\hbar} \end{aligned} \quad (1.6.17)$$

where the expansion,

$$\omega_\beta = \Psi_\beta - \langle \Psi_\alpha | \Psi_\beta \rangle_{R_{\beta\alpha}(t)} \quad (1.6.18)$$

has been used, and the ansatz made, that the global optical potentials ( $U$ : real part), and standard nucleon-nucleon interactions  $V$  fulfill the relation

$$\langle \Psi_\alpha | V_\alpha - U_\alpha | \Psi_\alpha \rangle = 0. \quad (1.6.19)$$

It is of notice that the overlap appearing in Eq. (1.6.18) can, in the case of a two-particle transfer reaction

$$\alpha \equiv a (= b + 2) + A \rightarrow b + B (= A + 2) \equiv \beta, \quad (1.6.20)$$

contribute with an amplitude  $\langle \Psi_\beta | \mathbb{1} | \Psi_\gamma \rangle \langle \Psi_\gamma | V_\alpha - U_\alpha | \Psi_\alpha \rangle$ , where  $\mathbb{1}$  is the unit operator, while  $\gamma \equiv f (= b + 1) + F (= A + 1)$ , denotes the mass partition of the

*italics*

intermediate channel. The above expression strongly suggests that a consistent description of two-transfer reactions in a non-orthogonal basis involves, at least, three strongly interwoven reaction channels (as testified by the fact that they can be shifted around by changing representation, that is post-post, prior-prior, and prior-post, see e.g. Eq. (1.6.2) as well as Fig. 5.C.2), namely  $\alpha$ ,  $\gamma$  and  $\beta$  and consequently has to be calculated, at least, to second order of perturbation theory, that is, including simultaneous and successive transfer and non-orthogonality corrections.

Let us now return to the sum-rule subject considering, for simplicity, the simultaneous transfer amplitude (1.6.17) (see also Sect. 5.C Eq.(5.C.4)). That is,

App.

$$a^{(1)}(t = +\infty) = \frac{1}{i\hbar} \int_{-\infty}^{\infty} dt \exp\left[\frac{i}{\hbar}(E^{bB} - E^{aA})t + \gamma_{\beta\alpha}(t)\right] \uparrow \uparrow \\ \times \langle \phi^{B(A)}(\mathbf{r}_{1A}, \mathbf{r}_{2A}) | U(r_{1b}) | e^{\sigma_{\beta\alpha}} \phi^{a(b)}(\mathbf{r}_{1b}, \mathbf{r}_{2b}) \rangle_{R_{\alpha\beta}(t)}, \quad (1.6.21)$$

where

$$\sigma_{\beta\alpha} = \frac{1}{\hbar} \frac{m_n}{m_A} (m_{aA} \mathbf{v}_{aA}(t) + m_{bB} \mathbf{v}_{bB}(t)) \cdot (\mathbf{r}_\alpha - \mathbf{r}_\beta), \quad (1.6.22)$$

takes care of recoil effects, the phase factor  $e^{\sigma_{\beta\alpha}}$  being a generalized Galilean transformation associated with the mismatch between entrance and exit channels, while the phase

$e^{i\sigma_{\beta\alpha}}$   
missing  
an  
imaginary  
unit

$$\gamma_{\beta\alpha}(t) = \int_0^t dt' \left\{ U_\beta(\mathbf{R}_\beta(t')) - \frac{1}{2} m_\beta v_\beta^2(t') - U_\alpha(\mathbf{R}_\alpha(t')) + \frac{1}{2} m_\alpha v_\alpha^2(t') \right\} \\ + \frac{1}{2\hbar} (m_\alpha \mathbf{v}_\alpha(t) + m_\beta \mathbf{v}_\beta(t)) \cdot (\mathbf{R}_\beta(t) - \mathbf{R}_\alpha(t)), \quad (1.6.23)$$

is related to the effective  $Q$ -value of the reaction.

The rate of change of the formfactor  $\langle \phi^{B(A)}, U(r_{1b}) e^{i\sigma_{\beta\alpha}} \phi^{a(b)} \rangle$  with time is slow, being completely overshadowed by the rapidly varying phase factor  $\exp\left[\frac{i}{\hbar}(E^{bB} - E^{aA})t + \gamma_{\beta\alpha}(t)\right]$ . Similar relations concerning recoil and  $Q$ -value effects can be obtained from the amplitudes associated to successive and to non-orthogonality terms i.e.  $a^{(2)}(\infty)$  and  $a^{(NO)}$  (see Ch. 5, Sect. 5.C).

Summing up, to compare two-nucleon transfer cross sections on equal structural footing, one has to eliminate the kinematical oscillating phase which can completely distort the “intrinsic” (reduced matrix element) value of the two-nucleon cross section. And for that, one has to work on each of the three amplitudes to extract at best the phases which couple relative and intrinsic motion.

Let us make a parallel with the sum rule associated with electromagnetic decay (Coulomb excitation,  $\gamma$ -decay). The absolute transition probability for absorption (emission) of a photon from nuclear dipole states is measured in  $\text{sec}^{-1}$  by (Bohr and Mottelson (1969))

$$T(E1) = (1.59 \times 10^{15}) \times (E)^3 \times B(E1), \quad (1.6.24)$$

where  $E$  is the energy of the transition and  $B(E1)$  the reduced transition probability. It is this quantity that enters the TRK-sum rule,

$$S(E1) = \langle 0 | [[H, \mathcal{M}(E1)], \mathcal{M}(E1)] | 0 \rangle / 2, \quad (1.6.25)$$

and not  $T(E1)$ . Now, in this particular case the  $Q$ -value dependence of the observed absolute transition probabilities can be eliminated analitically ( $E^3$  dependence), as well as the overall factor ( $1.59 \times 10^{15}$ ), in keeping with the fact that the mass partition ( $a + A \rightarrow a + A^*$ ) as well as the overall factor does not change between entrance and exit channels or, equivalently, the coordinate of relative motion  $\mathbf{R}_{\alpha\alpha'}(t)$  is always that describing the relative center of mass position of target and projectile. This fact allows for a complete separation between structure and reaction (kinematics), explicit in the general expression of  $T(E\lambda)$ , that is,

$$T(E\lambda; I_1 \rightarrow I_2) = \left( \frac{8\pi(\lambda+1)}{\lambda[(2\lambda+1)!!]^2} \frac{1}{\hbar} q^{2\lambda+1} \right) (B(E\lambda; I_1 \rightarrow I_2)), \quad (1.6.26)$$

where  $\mathbf{q}$  is the momentum of the photon, and

$$B(E\lambda; I_1 \rightarrow I_2) = \frac{\langle I_2 | \mathcal{M}(E\lambda) | I_1 \rangle}{\sqrt{2I_1 + 1}}, \quad (1.6.27)$$

the reduced transition probability. Thus, the first factor in the expression of  $T(E\lambda)$  contains all the kinematics (reaction) of the process, the second one the nuclear structure part of it. In the above relation, the multipole tensor is defined as,

$$\mathcal{M}(E\lambda, \mu) = \int \rho(\mathbf{r}) r^\lambda Y_{\lambda\mu}(\hat{\mathbf{r}}) d\mathbf{r}. \quad (1.6.28)$$

It is of notice that the non-diagonal elements (transition moments) are involved in electric  $\rho_e$  and nuclear ( $\rho$ ) multipole processes ( $\gamma$ -decay, Coulomb excitation, inelastic scattering, etc.).

Returning to the expression of the first order (simultaneous) two-nucleon transfer amplitude  $a^{(1)}(t = +\infty)$  one can only devise empirical protocols to try to extract the  $\gamma$ - and  $\sigma$ -phase dependence (see Eqs. (1.6.21)–(1.6.23)) from it and set all absolute two-nucleon transfer cross sections  $d\sigma/d\Omega \sim |a|^2$  on equal footing regarding kinematics, so as to allow to compare the intrinsic, reduced transition probabilities (structure). In other words, extract the structure information contained in, e.g.,

$$\phi^{B(A)}(\mathbf{r}_{1A}, \mathbf{r}_{2A}) = \langle \mathbf{r}_{1A}, \mathbf{r}_{2A} | \Gamma_1^\dagger(\beta = +2) | \tilde{0} \rangle, \quad (1.6.29)$$

where

$$\Gamma_n^\dagger(\beta = +2) = \sum_k X_k^n [a_k^\dagger a_k^\dagger]_0 - \sum_i Y_i^n [a_i a_i]_0, \quad (1.6.30)$$

is the pair creation addition mode acting on of a closed shell system  $|\tilde{0}\rangle$ , as well as in

$$\phi^{B(A)}(\mathbf{r}_{1A}, \mathbf{r}_{2A}) = \langle \mathbf{r}_{1A}, \mathbf{r}_{2A} | [a_k^\dagger a_k^\dagger]_0 | 0 \rangle, \quad (1.6.31)$$

 different